Journal of Materials Processing Technology 245 (2017) 167–179

Contents lists available at ScienceDirect

Journal of Materials Processing Technology

journal homepage: www.elsevier.com/locate/jmatprotec

Estimation of filament temperature and adhesion development in fused deposition techniques

S.F. Costa [a], F.M. Duarte [b], J.A. Covas [b,*]

[a] CIICESI—Center for Research and Innovation in Business Sciences and Information Systems, School of Management and Technology (ESTGF) of Porto Polytechnic Institute (IPP), 4610-156 Felgueiras, Portugal
[b] I3N/IPC—Institute for Polymers and Composites, Department of Polymer Engineering, University of Minho, 4800-058 Guimarães, Portugal

ARTICLE INFO

Article history:
Received 3 October 2016
Received in revised form 11 January 2017
Accepted 26 February 2017
Available online 28 February 2017

Keywords:
Fused deposition techniques
Heat transfer modelling
Adhesion

ABSTRACT

This work presents an analytical solution to the transient heat conduction developing during filament deposition in Fused Deposition Techniques (FDT), which is coupled to a routine that activates or deactivates all relevant local boundary conditions depending on part geometry, operating conditions and deposition strategy. Boundary conditions include contact between filament segments, between filament segments and the support, as well as heat transfer with the environment. The resulting MatLab code comprises an adhesion criterion that is used to estimate whether contiguous filament segments will adhere adequately to each other prior to solidification. Predicted and experimental data for the filament surface temperature showed very good agreement. Also, adhesion predictions were in accordance with the results of real peel-like tests. The practical potential of this calculation tool is demonstrated by an application example.

1. Introduction

As defined by the ASTM: F2792 – 12a (2012) standard, Additive Manufacture is the "process of joining materials to make objects from 3D model data, usually layer upon layer, as opposed to subtractive manufacturing methodologies, such as traditional machining". Among the various available processes, fused deposition techniques (FDT) – comprising Fused Deposition Modelling (FDM) and Free Form Extrusion (FFE) – are popular due to their easy operation, reproducibility, low cost and ability to accept sustainable materials (Chua et al., 2010).

Their *modus operandi* consists in pushing a plastic rod through a heated die and depositing the molten extruded thin filament onto the support as a vertical series of horizontal 2D slices of a 3D part. This makes FDT appropriate for a wide range of applications, such as functional prototyping, rapid tooling (Ingole et al., 2009) and the manufacture of short series of parts for engineering applications, e.g., for the automotive and medical industries (Masood, 2014).

Products made by FDT can vary significantly in quality, depending on operation parameters, machine specifications, material properties and part geometry (Villalpando et al., 2014). Several studies focused the optimization of surface finish, dimensional accuracy and mechanical strength. Galantucci et al. (2009) monitored the influence of FDM process parameters on the surface finish of acrylonitrile butadiene styrene (ABS) parts. They concluded that slice height and filament width are the most important variables. Boschetto et al. (2013) and Boschetto and Bottini (2016) predicted the surface roughness of FDM parts as a function of process parameters. As for the mechanical performance, Ahn et al. (2002) found out that the distance between filaments and filament orientation greatly influence the tensile strength of a printed part. In turn, Sood et al. (2010) showed that distortions within or between layers, thick filaments and excessive number of layers contribute to higher residual stresses, i.e., to a deterioration of the resistance. Croccolo et al. (2013) developed an analytical model predicting the strength and the stiffness of specimens shaped according to the ASTM D638-10 standard. Comparison with experimental data showed differences of approximately 4%.

During deposition, filament deformation and bonding between contiguous filament segments are prevailing process variables (Villalpando et al., 2014). Céline et al. (2004) estimated the dynamics of bond formation from sintering data of ABS filaments. Sun et al. (2008) and Gurrala and Regalla (2014) analyzed changes in the mesostructure and degree of healing at the interfaces between adjoining polymer filaments. They concluded that fabrication strategy, environment temperature and variations in convection determine the overall quality of the bond strength. Once deposited,

* Corresponding author.
E-mail addresses: sfc@estgf.ipp.pt (S.F. Costa), fduarte@dep.uminho.pt (F.M. Duarte), jcovas@dep.uminho.pt (J.A. Covas).

http://dx.doi.org/10.1016/j.jmatprotec.2017.02.026
0924-0136/

Nomenclature

$T_r\,(x,t)$	Temperature (°C) at location x and time t of the r^{th} filament segment (($r \in \{1, \ldots, N\}\{1,\ldots,N\}$, where N is the total number of filament segments required to build the part
T_{r_i}	Temperature (°C) of the filament segment or support in contact with the r^{th} filament segment i ($r_i \in \{1,\ldots, N+1\}$, $r_i \neq r$).
T_r	Filament temperature at time $t_r\,(x)$ (°C)
T_E	Environment temperature (°C)
k	Thermal conductivity (W/m °C)
ρ	Specific weight (kg/m^3)
C	Specific heat capacity (J/kg °C)
h_{conv}	Convective heat transfer coefficient (W/m^2 °C)
h_i	Heat transfer coefficient for contact $i \in \{1,\ldots,n\}$ (W/m^2 °C)
n	Number of physical contacts with adjacent filament segments or with support
A	Area of filament cross-section (m^2)
A_{rconv}	Area exposed to the environment (m^2)
A_{ri}	Area of contact i for the r^{th} filament (m^2)
P	Filament perimeter (m),
λ_i	Fraction of P
$t_r(x)$	Time at which an elementary length x (s) of the rth filament segment is deposited (s)
$t_w(T)$	Welding time (s)
v_{air}	Air velocity (m/s)
μ_{air}	Air viscosity (Pa)
Δt	Time increment (s)
μ	Convergence error (°C)
ρ_{air}	Air specific weight (kg/m^3)

each filament segment should solidify as quickly as possible to avoid excessive deformation due to gravity and/or the weight of the material deposited above it; conversely, it should remain sufficiently hot during enough time to ensure adequate bonding with the neighbouring filament segment(s). Also, during cooling shrinkage and residual stresses develop, which may induce warping and delamination (Kantaros and Karalekas, 2013). Thus, it is important to know the evolution of filament temperature during deposition and cooling and how it is affected by process parameters.

Yardimci and Güçeri (1996) and Yardimci et al. (1997) modelled the cooling of a filament due to convection with the environment (i.e., disregarding contacts with adjacent segments) and showed the effect of adopting different build strategies. Li (2002) approached the same problem by coupling a lumped capacity method to a 1D analytical transient heat transfer analysis of a single filament with an elliptical cross-section. Rodriguez et al. (2000) and Rodriguez et al. (2003) developed a 2-D transient heat transfer analysis of the solidification of a rectangular filament in a vertical stack, also neglecting all contact resistances. Bonding was predicted using a wetting-diffusion model based on the reptation theory and it was shown that lower cooling rates promote stronger bonding. Bellini and Güçeri (2003) and Bellini et al. (2005) used ANSYS POLYFLOW (a general purpose finite-element-based software) to model the extrusion, deposition and cooling stages of FDM, taking into consideration heat exchanges with the surroundings, between filament segments and between filament and support.

Recently, the authors, Costa et al. (2015) examined the contribution of various thermal phenomena developing during FDT to the overall heat transfer, including convection and radiation with the environment, conduction with support and between adjacent filament segments, radiation between adjacent filament segments and convection with entrapped air. The magnitude of the mechanical deformation was also studied. It was experimentally demonstrated that during the deposition step heat exchanges by convection with the environment, by conduction between adjacent filament segments and by conduction with the support are relevant in terms of temperature evolution. It was also shown that: (i) temperatures in any filament cross-section are relatively uniform except when thermal contacts are perfect and that (ii) under normal operating conditions the total mechanical deformation of the filament is small and, consequently, its influence on heat transfer and dimensional accuracy of the part is negligible. In this work, an analytical solution for the transient heat transfer during filament deposition and cooling is proposed, taking into consideration all physical contacts between filament segments during the progressive built-up of a 3D structure. Furthermore, the analysis is coupled to an adhesion quality assessment criterion, thus yielding a computational code that can predict the time evolution of filament temperature as well as the bond quality between all adjacent filament segments of a 3D part. The predictions are assessed experimentally.

2. Heat transfer during filament deposition

In FDT, the extruded filament is subjected to a specific heat transfer mechanism, but with boundary conditions changing as the deposition progresses. The following nomenclature is adopted here: (i) *filament* refers to the total length of extrudate used to manufacture the part ; (ii) *filament segment* denotes a length of filament that is deposited by the machine nozzle in one horizontal plan before reversing the deposition direction (thus, each plan is typically built by a series of parallel filament segments, an exception being spiral deposition, which involves a single filament segment); (iii) *elementary lengths* of any filament segment are gradually deposited. In general, the energy balance for an elementary length dx can be written as:

$$\begin{cases} \textit{Energy in at one face} - \textit{Heat transfer by convection with environment} \\ -\textit{Heat transfer by conduction between adjacent filament segments or} \\ \textit{support} \end{cases} = \textit{Change in internal energy} + \textit{Energy out at opposite face}$$

Mathematically:

$$-kA\frac{\partial T_r(x,t)}{\partial x} - h_{conv}(A_r)_{conv}\left(T_r(x,t) - T_E\right) - \sum_{i=1}^{n} h_i(A_r)_i\left(T_r(x,t) - T_{r_i}\right) = \\ = \rho CA\frac{\partial T_r(x,t)}{\partial t}dx - A\left[k\frac{\partial T_r(x,t)}{\partial x} + \frac{\partial\left(k\frac{\partial T_r(x,t)}{\partial x}\right)}{\partial x}dx\right] \quad (1)$$

where:

$T_r(x,t)$ – Temperature (°C) at location x and time t of the r^{th} filament segment (($r \in \{1, \ldots, N\}\{1,\ldots,N\}$, where N is the total number of filament segments required to build the part

Tr_i – Temperature (°C) of the filament segment or support in contact with the r^{th} filament segment i ($r_i \in \{1,\ldots, N+1\}$, $r_i \neq r$).

T_E – Environment temperature (°C)

k – Thermal conductivity (W/m °C)

ρ – Specific weight (kg/m^3)

C – Specific heat capacity (J/kg °C)

h_{conv} – Convective heat transfer coefficient (W/m^2 °C)

h_i – Heat transfer coefficient for contact $i \in \{1,\ldots,n\}$ (W/m^2 °C)

n – Number of physical contacts with adjacent filament segments or with support

A – Area of filament cross-section (m^2)

$(A_r)_{conv}$ – Area exposed to the environment (m^2)

$(A_r)_i$ – Area of contact i for the r^{th} filament (m^2) – see Fig. 1 for an identification of possible contact areas and heat transfer modes

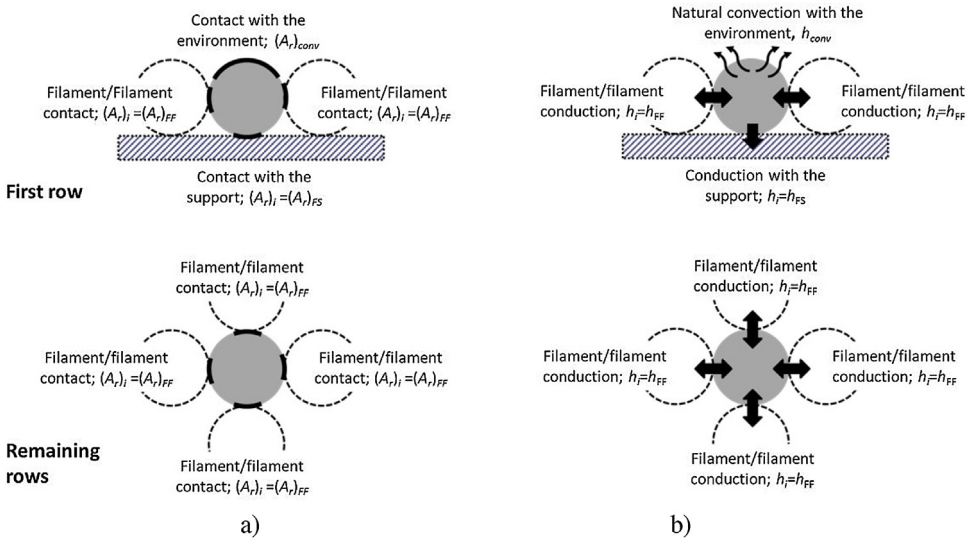

Fig. 1. Possible contact areas (a) and heat transfer modes (b) for a filament segment (in grey).

with:

$$(A_r)_i = Pa_{r_i}\,\lambda_i dx,\ i \in \{1,\cdots,n\},\ (A_r)_{conv} = \mathrm{P}\left(1-\sum_{i=1}^{n} a_{r_i}\lambda_i\right)\mathrm{dx} \tag{2}$$

In these expressions, P is the filament perimeter (m), λ_i is the fraction of P that is in contact with another filament segment or with the support and a_{r_i} is a variable defined as:

$$a_{r_i} = \begin{cases} 1 \text{ if ther}^{th}\text{filament has the } i^{th}\text{contact} \\ \\ 0 \text{ otherwise} \end{cases}, \forall i \in \{1,\ldots,n\}, \forall r \in \{1,\ldots,N\} \tag{3}$$

Using Eq. (2), (1) can be re-written as:

$$\frac{\partial T_r(x,t)}{\partial t} = \frac{k}{\rho C}\frac{\partial^2 T_r(x,t)}{\partial x^2} - \frac{P}{\rho CA}\left(h_{conv}\left(1-\sum_{i=1}^{n} a_{r_i}\lambda_i\right)\left(T_r(x,t)-T_E\right)+\sum_{i=1}^{n} h_i a_{r_i}\lambda_i\left(T_r(x,t)-T_{r_i}\right)\right) \tag{4}$$

which shows that the evolution of the filament temperature is governed by:

- Axial conduction, controlled by $\frac{k}{\rho C}$;
- Convection with the environment, ruled by $\frac{Ph_{conv}}{\rho CA}$;
- Conduction between adjacent filament sections, proportional to $\frac{Ph_i}{\rho CA}$.

Given the low thermal conductivity of most polymers and the small filament diameter (smaller than 1 mm), axial heat conduction can be neglected when compared with the remaining (Costa et al., 2015). Therefore, Eq. (4) reduces to:

$$\frac{\partial T_r(x,t)}{\partial t} = -\frac{P}{\rho CA}\left(h_{conv}\left(1-\sum_{i=1}^{n} a_{r_i}\lambda_i\right)\left(T_r(x,t)-T_E\right) + \sum_{i=1}^{n} h_i a_{r_i}\lambda_i\left(T_r(x,t)-T_{r_i}\right)\right) \tag{5}$$

Using the characteristic polynomial method (Palais and Palais, 2009), Eq. (5) can be solved analytically to yield the evolution in time of the filament temperature:

$$T_r(x,t) = C_1 \exp\left[\frac{-Pb\left(a_{r_1},\ldots,a_{r_n}\right)}{\rho CA}\left(t-t_r(x)\right)\right] + Q\left(a_{r_1},\ldots,a_{r_n}\right). \tag{6}$$

where $t_r(x)$ is the time at which an elementary length x of the r^{th} filament segment is deposited and, consequently, begins to cool down or contacts an adjacent filament segment or the support, and C_1 is defined as:

$$C_1 = T_r\left(t_r(x)\right) - Q\left(a_{r_1},\ldots,a_{r_n}\right). \tag{7}$$

Here, (T_r) is the filament temperature at time $t_r(x)$. Functions $b\left(a_{r_1},\ldots,a_{r_n}\right)$ and $Q\left(a_{r_1},\ldots,a_{r_n}\right)$ depend on the existing contacts:

$$b\left(a_{r_1},\ldots,a_{r_n}\right) = h_{conv}\left(1-\sum_{i=1}^{n} a_{r_i}\lambda_i\right) + \sum_{i=1}^{n} a_{r_i}h_i\lambda_i \tag{8}$$

$$Q\left(a_{r_1},\ldots,a_{r_n}\right) = \frac{h_{conv}\left(1-\sum_{i=1}^{n} a_{r_i}\lambda_i\right)T_E + \sum_{i=1}^{n} a_{r_i}h_i\lambda_i T_{r_i}}{b\left(a_{r_1},\ldots,a_{r_n}\right)} \tag{9}$$

The Biot number is defined as Bejan (1993)

$$Bi = \frac{A}{P}\frac{b\left(a_{r_1},\ldots,a_{r_n}\right)}{k} \tag{10}$$

If Bi <0.1, temperature gradients in each filament cross-section can be neglected and so the assumption of uniform temperature at each cross-section remains valid.

3. Adhesion criterion

The operating conditions of FDT should be selected in such a way that contiguous filament segments adhere adequately to each other before solidifying. Based on the diffusion theory, Yang and Pitchumani (2002) proposed an expression for the evolution of the degree of healing $D_h(t)$ between two contacting rods:

$$D_h(t) = \left[\int_0^t \frac{1}{t_w(T)}dt\right]^{1/4}, \tag{11}$$

where $t_w(T)$ is the welding time. This approach was successfully applied by Sun (2004) to predict the degree of healing between adjacent filament segments in FDM and consequently it will be adopted here. Using available experimental data from the literature for an Acrylonitrile Butadiene Styrene (ABS) (Rodriguez et al., 2000), Sun (2004) obtained the following relationship for t_w:

$$t_w = 1.080 \times 10^{-47} \exp\left(\frac{Q_d}{RT}\right), \quad (12)$$

where $Q_d = 388.7$ kJ/mol and R is the universal gas constant.

4. Modeling of filament deposition

Eq. (6) describes the evolution with time of the temperature of a filament segment at any cross-section along its length x. The gradual deposition of a filament segment is modeled by considering a series of adjoining elementary lengths, each associated to a given deposition time. The type of contacts existing in each length must be defined (contact with the support, contact with previously deposited element(s), or exposure to the environment). Then, the temperature at each time increment is calculated for all the existing elementary lengths, until the deposition is completed. The calculations comprise the following steps:

a) Discretization of time and updating the thermal conditions

At each time increment Δt, an elementary length of the filament segment is deposited. Thus, as successive values of Δt are taken in, the length of the filament segment deposited increases. The value of Δt should ensure a good balance between computation time and sufficient accuracy. For example, considering a sequence of two layers of four filament segments, Fig. 2 shows the time evolution of the temperature of filament segment 1, at $x = 0.00125$ m, for different values of Δt. A typical extrusion velocity of 0.025 m/s, an extrusion temperature of 270 °C and ABS material properties were assumed. The fraction of perimeter for contact with support, at the right and upper sides of the filament were 0.30, 0.20 and 0.30, respectively. The predictions become coincident for $\Delta t \leq 0.2$ s. Practice showed that Δt should be smaller or equal to the ratio between the cross-section A and the deposition velocity v:

$$\Delta t \leq \frac{A}{v} \quad (13)$$

b) Building strategy

The building strategy determines the type of contacts taking place (these are identified in Fig. 1). Unidirectional and aligned, unidirectional and skewed, and perpendicular deposition modes were considered in the calculations (Fig. 3). In turn, the sequence of contacts will be determined by the geometry of the part.

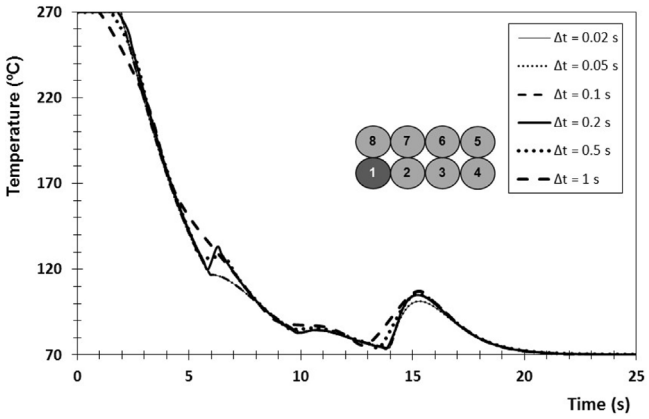

Fig. 2. Time evolution of the temperature of filament segment 1 for a sequence of 8 filament segments deposited at $v = 0.025$ m/s, for various values of time intervals, Δt.

c) Computation of filament temperature

During building of the part, a filament segment already laid down will be reheated upon contact with a newer one that is hotter, whilst a segment contacting previously deposited neighbours will cool down faster than if exclusively due to convection. Taking these events into consideration implies the simultaneous computation of the temperature of all the filament segments deposited up to a given time, for the thermal boundary conditions updated as explained above.

d) Adhesion

At any part location, $D_h(t)$ (Eq. (11)) is computed while the filament temperature is higher than its glass transition temperature, T_g, and also while its value remains lower than unity (threshold for good adhesion). During the calculations, since when $D_h(t) \leq 1$ the thermal resistance is high, the elementary lengths of filament segment in contact are considered as distinct bodies. When and if $D_h(t) > 1$, the thermal contact conductance is high and the interfacial temperature is taken as the average of the temperatures of the two elements. The equation is solved using the trapezoidal method.

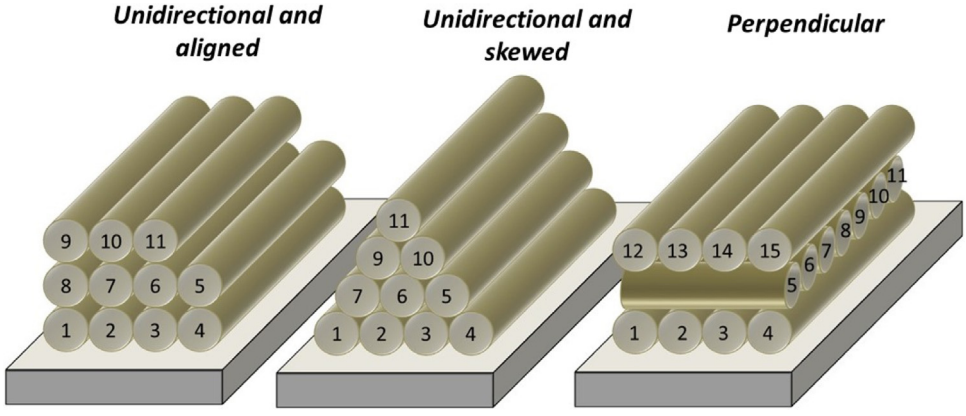

Fig. 3. Building strategies considered in the calculations.

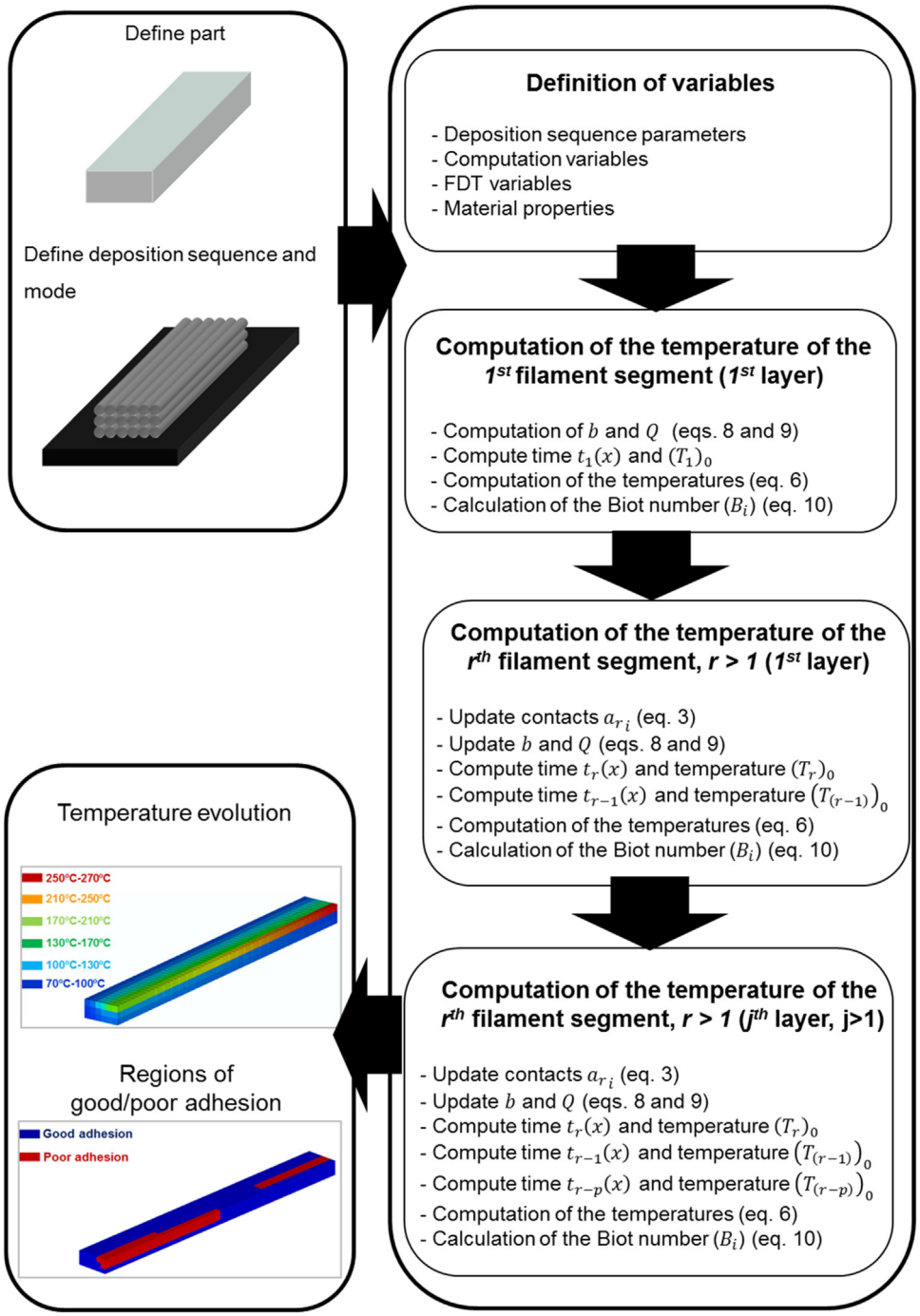

Fig. 4. Flowchart of the computer code.

e) Code

A MatLab® code was developed in accordance with the flowchart presented in Fig. 4. The program yields the temperature evolution and resulting degree of adhesion at any location of a part. The user defines the geometry of the part, the building strategy and the deposition sequence (the input data includes the number of layers, the number of filament segments and the fraction of perimeter of the filament section in contact with another segment, with the support and with the environment, respectively). The extrusion conditions (extrusion temperature and velocity, environment temperature) and the thermal properties (heat transfer coefficients, thermal contact conductance) must also be input.

The temperature computations are carried out in three main steps. Calculations start with the first layer. The first filament segment develops contacts exclusively with the support and with the environment. For the remaining filament segments of the first row, contacts with adjacent filament segments arise. In the case of filament segments of the remaining rows, contacts with neighbouring segments and with the environment occur.

In every step, the time at which filament segment r is deposited, $t_r(x)$, as well as its initial temperature, $(T_r)_0$, are calculated, together with the time and temperature of previously deposited filament segments in contact (when applicable), i.e., $t_{r-1}(x)$, $t_{r-p}(x)$, $\left(T_{(r-1)}\right)_0$ and $\left(T_{(r-p)}\right)_0$. When two filament segments are in contact, the computation of $T_1(x,t + \Delta t)$ requires the value of $T_2(x,t+\Delta t)$,

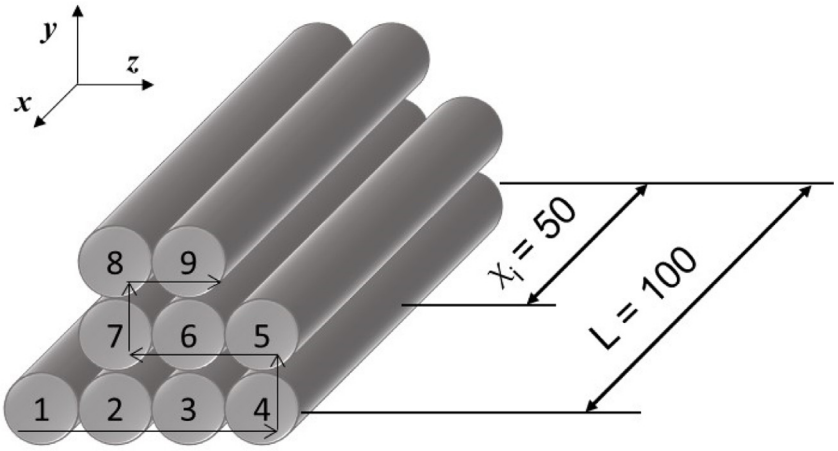

Fig. 5. Geometry and deposition sequence used to illustrate the results of the calculations (dimensions in mm).

Table 1
Process parameters and material properties.

Property	Value
Extrusion temperature (°C)	270
Environment temperature (°C)	70
Extrusion velocity (m/s)	0.025
Cross-section diameter (m)	0.000359
Fraction of perimeter for contact at right side	0.2
Fraction of perimeter for remaining contacts	0.1
Heat transfer coefficient (convection) (W/m^2 °C)	70
Heat transfer coefficient (conduction) between filament segment and support (W/m^2 °C)	300
Heat transfer coefficient (conduction) between filament segments (W/m^2 °C)	70
Thermal conductivity (W/m°C)	0.1768
Specific heat (J/kg°C)	2019.7
Specific weight (kg/m^3)	1050

Table 2
Material properties of ABS FA 4475.

Property	Value
Specific weight (kg/m^3)	1050
Thermal conductivity (W/m °C)	0.18
Specific heat (J/kg °C)	2200
Emissivity	0.85 ± 0.01
MFI (g/10 min) @ 220 °C–10 kg	34

which is unknown, hence an iterative process with a convergence error, μ (°C), is applied. All constants related with contact (e.g., contact area, a_{ri}) and constants b and Q are updated at each time increment. Finally, the Biot number is determined to check if the assumption of uniform temperature at each cross-section remains valid.

The code generates a data file yielding the temperature evolution during the time defined by the user (typically including deposition and cooling) together with the time required for adequate adhesion between adjacent filament elements.

To exemplify the results produced, the simple geometry and deposition sequence illustrated in Fig. 5 are considered, together with the process parameters and material properties presented in Table 1. The thermal properties were taken from the literature (Rodriguez et al., 2000).

Fig. 6 shows the filament temperature at various instants of the deposition process (an animated view of cooling can be created). Clearly, the newest filament segment or elementary length is always the hottest one and cools down gradually, although the effect of the physical contacts is difficult to perceive in this representation. The phenomenon is better seen in Fig. 7, which depicts the time evolution of the temperature of filament segments 1–9 at a vertical *xx* plan distant 0.05 m from the origin (see Fig. 5). As a new filament segment is deposited, the temperature of the adjacent segments increases and so their cooling is delayed. The physical contacts can alter local filament temperatures by as much as 18 °C.

Fig. 8 depicts the predicted contact time required for good adhesion between all pairs of touching filament segments, for three different extrusion temperatures. The dotted bars correspond to $D_h(t) \leq 1$ (Eq. (11)), i.e., to insufficient adhesion. In general, the healing time is very short, typically less than 0.25 s. For example, at 230 °C there is no adhesion between pair 1&2 (the two oldest filament segments), rapid adhesion between pair 2&3 and no adhesion for 3&4. Due to the limited heat transfer between segments 1 and 2, the latter retains sufficient temperature to adhere to segment 3 when this becomes into contact. This increases the rate of cooling of segment 3, which will not be able to adhere to segment 4.

5. Experimental

5.1. Materials

An Acrylonitrile-Butadiene-Styrene (ABS FA 4475, Poliversal, Portugal) amorphous polymer, with the properties shown in Table 2, was used in the experiments. The emissivity was obtained by heating a sample in a hot plate (Selecta Combinax) to various temperatures within the range of interest, each time measuring its surface temperature by a fast reading type K thermocouple (Digital Handheld Thermometer, Anritsu, HFT-80) and by an infrared FLIR SC640 camera. The emissivity was then determined using the ThermaCAM Researcher Pro 2.8 SR-2® software, by inserting emissivity values until the two temperatures coincided.

5.2. Equipment layout

The experimental set-up used to perform the experimental work is presented in Fig. 9. It comprises a prototype mini-single screw extruder (screw diameter, ø = 12 mm) (Teixeira et al., 2015) coupled to a melt gear pump (Extertal Lenze 32699, Germany), in order to ensure a stable output. The circular die (ø = 1 mm) was designed to extrude vertically downwards a filament whose temperature can be measured by thermography. This filament was deposited on a 3D table actuated by 3 independent step motors with an accuracy of 0.05 mm, controlled by CAD/CAM software. The maximum displacement in the *x* and *y* directions is 150 mm and in the *z* direction

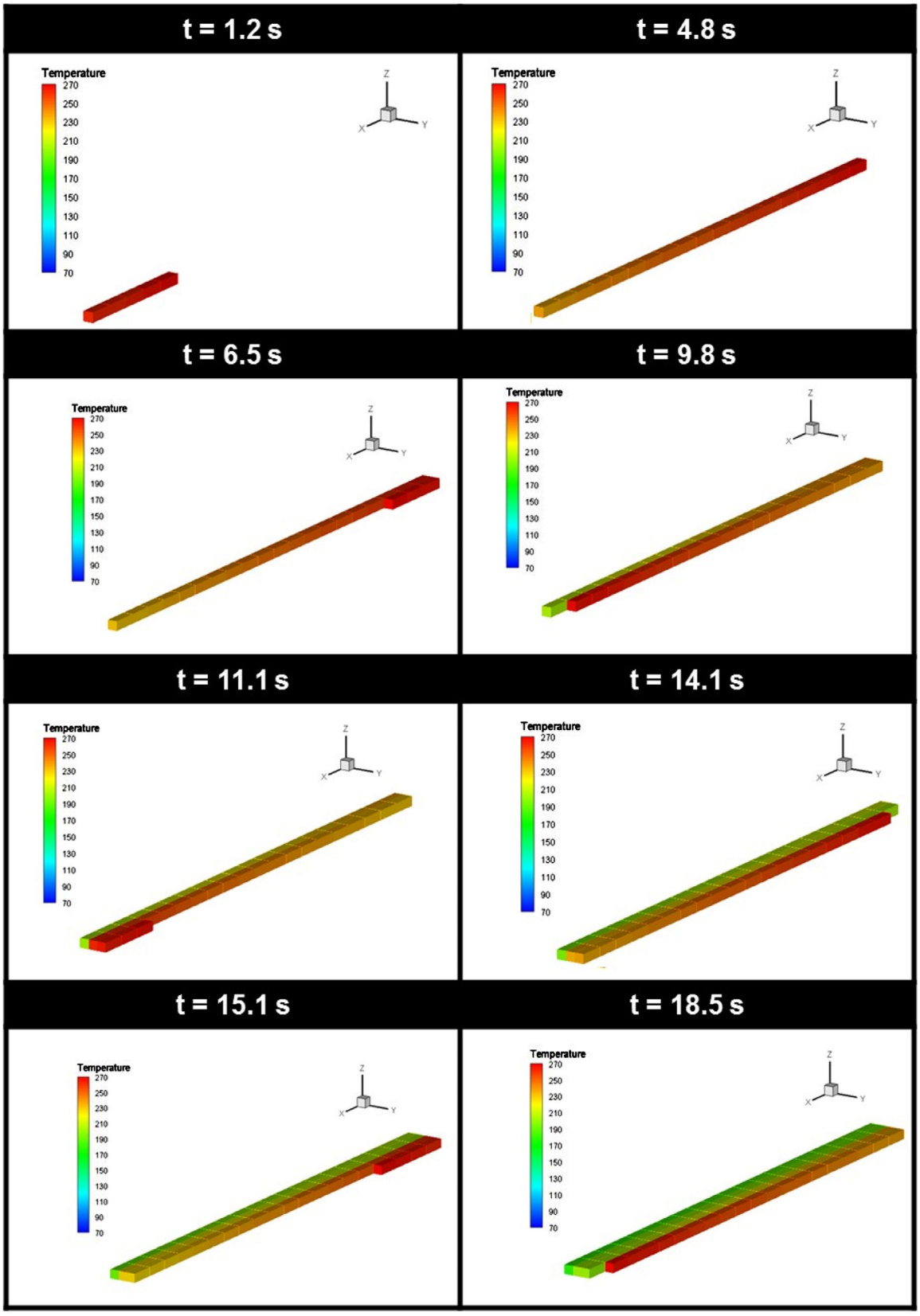

Fig. 6. Filament temperature at various instants of the deposition process.

is 100 mm. The surface temperature of the filament was recorded by an infrared FLIR ThermaCAM SC640 camera positioned above the extrusion head, by means of the ThermaCAM Researcher Pro 2.8 SR-2® software.

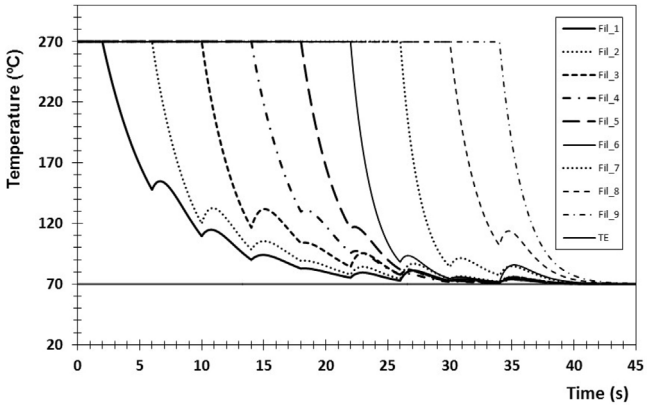

Fig. 7. Time evolution of the temperature of filament segments 1–9 for the geometry and deposition sequence illustrated in Fig. 5, at a vertical *xx* plan distant 0.05 m from the origin.

Table 3
Extrusion conditions.

Variable	Value
Filament temperature at die exit	190 °C (die set to 200 °C) 210 °C (die set to 220 °C)
Temperature surrounding the 3D table	40 °C–65 °C (depending on the distance to the extruder)
Extruder screw speed	14 rpm
Deposition Velocity	0.015 m/s

5.3. Experimental procedure

The filament was extruded under the conditions presented in Table 3. The displacement rate of the 3D table was adjusted to match the linear velocity of the extrudate (which was set to a low value in order to facilitate the measurements). Thermal images with a frequency of 7.5 Hz were recorded by the infrared camera until approximately 120 s after deposition had been completed (Table 4 shows the input parameters of the thermal camera software). In order to correlate the deposition parameters with adhesion upon the development of thermal contacts, the deposition patterns illustrated in Fig. 10 were performed for two extrusion temperatures (see Table 3). A peel-like test was performed by pulling apart under a fixed load the two ends of the filament. The surviving contact length, B_p, was taken as a measure of adhesion strength.

Table 4
Input parameters for the ThermaCAM Researcher Pro2.8 SR-2® software.

Variable	Value
Ambient controlled temperature	23 °C
Temperature surrounding the extruder	40 °C–65 °C
Distance between camera and support table	1 m
Emissivity	0.85

Since the filament is essentially a cylindrical body, the coefficient of heat transfer between filament and the surroundings, h_{conv}, was determined using the Hilpert correlation (Bejan, 1993):

$$h_{conv} = \frac{Nu_d \cdot k}{d} \tag{15}$$

where d is the diameter (m), k is the thermal conductivity (W/m °C) and Nu_d is the Nusselt number defined by:

$$Nu_d = C_H \cdot Re^{n_H} \cdot Pr^{1/3}. \tag{16}$$

In this expression, Re is the Reynolds number, C_H and n_H are empirical constants estimated from Hilpert's data (Bejan, 1993) and Pr is the Prandtl number at the environment temperature, T_E (°C). The Reynolds number is expressed as:

$$Re = \frac{\rho_{air} \cdot v_{air} \cdot d}{\mu_{air}} \tag{17}$$

where μ_{air} is the air viscosity (Pa) at T_E, v_{air} is the air velocity (m/s) and ρ_{air} is the air specific weight (kg/m^3). Thus, use of Eq. (15) requires knowledge of the filament cross-section, air velocity and air temperature. By machining a slot on the table support, a 5 mm long filament portion became subjected exclusively to convection. Its cross-section was determined using a Stereoscopic Olympus Magnifier and the Leica Qwin V3 Software, the air temperature was measured with a type K thermocouple (Hanna Instruments) and

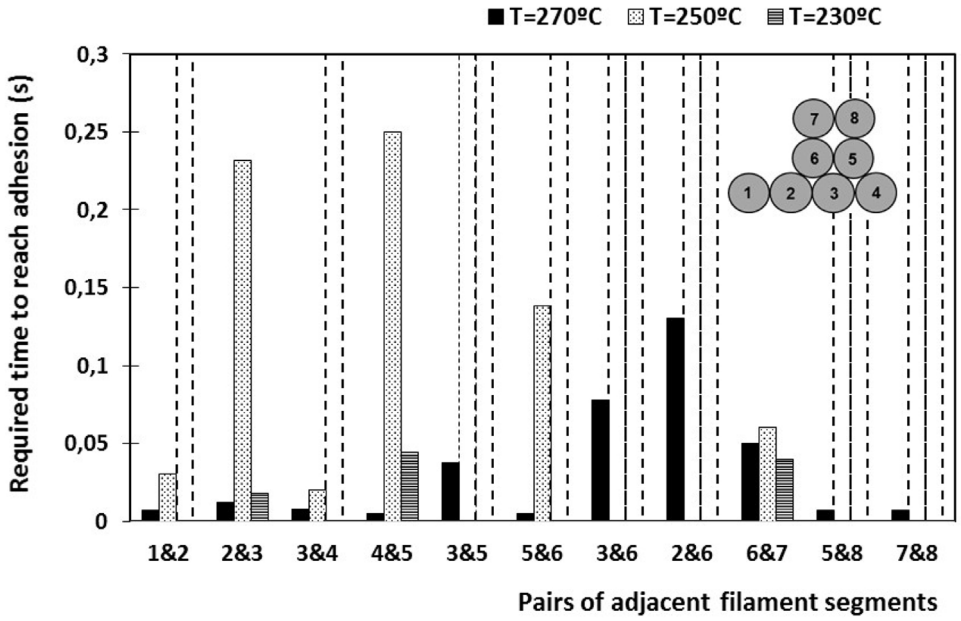

Fig. 8. Time required to achieve good adhesion between pairs of adjacent filament segments for the geometry and deposition sequence illustrated in Fig. 5, at a vertical *xx* plan distant 0.05 m from the origin.

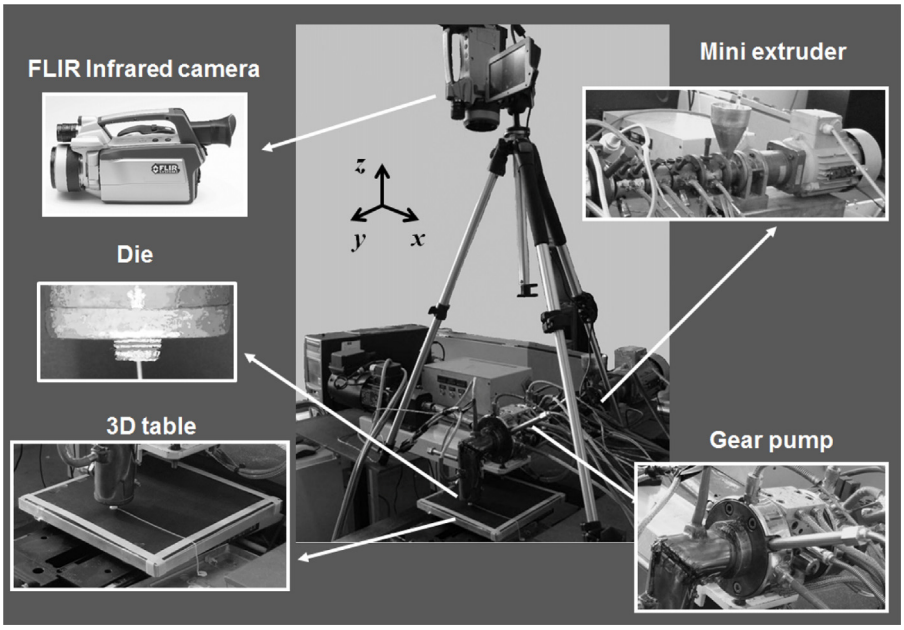

Fig. 9. Experimental set-up.

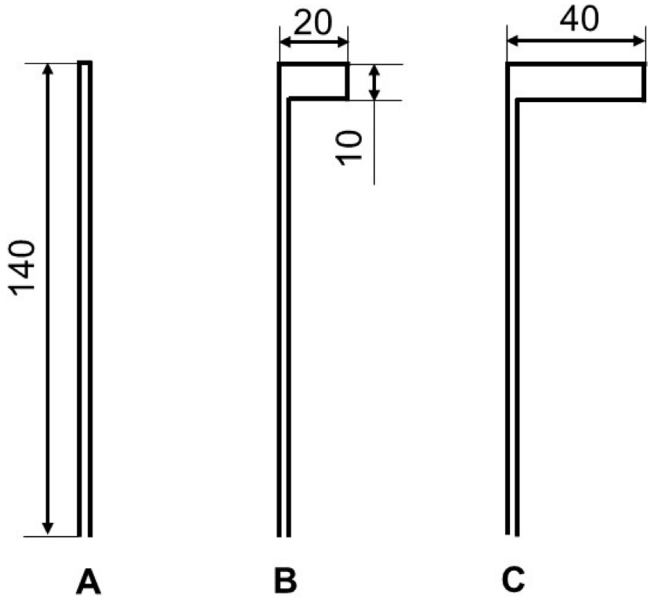

Fig. 10. Deposition patterns for evaluation of adhesion strength (dimensions in mm).

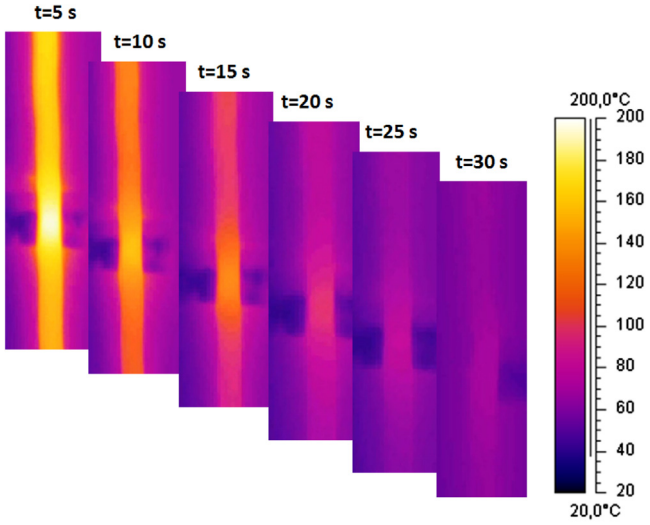

Fig. 11. Typical IR images of the evolution of filament temperature with time.

the air velocity with a digital anemometer (TES-1340). The calculated and measured values of filament temperature when only heat transfer by convection develops were made to coincide by adjusting h_{conv}. To estimate the coefficient of heat transfer by conduction between filament and support, h_{FS}, the temperature evolution of the filament where contact with the support exists, the cross-section of the filament and the contact area between filament and support were measured. Then, calculated and actual temperatures were made to overlap by adjusting h_{FS}. In the case of the coefficient of heat transfer by conduction between filaments, h_{FF}, the temperature evolution of two overlapping filament segments was registered, together with their cross-sections, mutual contact area and contact area of the bottom segment with the support. In the temperature computations, the values of h_{conv} and h_{FS} previously determined were utilized.

6. Results and discussion

6.1. Heat transfer coefficients

Fig. 11 shows a typical IR image of the evolution of filament temperature with time upon deposition onto the support containing a transversal slot, with the objective of determining h_{conv} as explained in the preceding section. Both the air temperature in the slot and the local filament temperatures are clearly detected. For air velocity, v_{air}, in the surroundings of the 3D table ranging between 0.3 and 0.5 m/s, h_{conv} was estimated to vary between 52 W/m^2 °C and 62 W/m^2 °C, respectively. This compares satisfactorily with the value of 67 W/m^2 °C obtained by Rodriguez et al. (2000) using the Churchill correlation for natural convection for an elliptical filament extruded at 270 °C into an environment at 70 °C. Sun (2004) assumed that h_{conv} may vary in the range 10–140 W/m^2 °C. Fig. 12 pertains to the determination of the thermal contact conductance, h_{FS}. Assuming h_{conv} = 62 W/m^2 °C and using in the calculations the filament diameter and the contact area determined experimentally

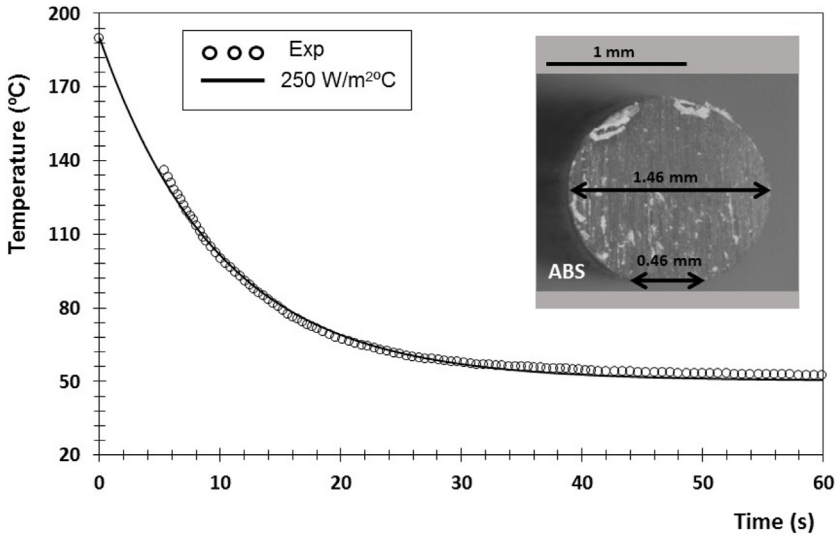

Fig. 12. Determination of h_{FS}: evolution of filament temperature with time at $x = 40$ mm (die set to 200 °C).

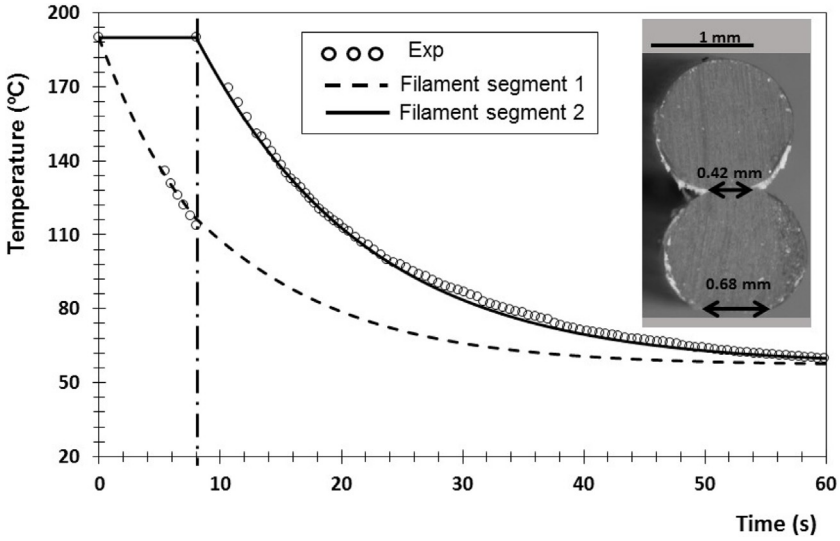

Fig. 13. Determination of h_{FF}: evolution of temperature with time at $x = 40$ mm of two filament segments deposited on top of each other (die set at 200 °C).

(see photo inset), the overlap of the predicted and experimental temperatures yielded $h_{FS} = 250\ W/m^2\ °C$. A matching superposition was obtained for the two extrusion temperatures. As expected, $h_{FS} > h_{conv}$, i.e., filament locations in contact with the support cool down faster.

The evolution of temperature (at $x = 40$ mm and for the extrusion die set to 200 °C) of two filament segments deposited on top of each other, together with their cross-sections after cooling, is shown in Fig. 13. The segment at the bottom was laid down moving the support in one direction, while the segment on top was deposited moving the support in the opposite direction. The vertical line identifies the instant when contact begins. Excellent agreement between measurements and predictions was obtained when $h_{FF} = 50\ W/m^2\ °C$. It is interesting to note that $h_{FF} < h_{FS,}$ i.e., that the cooling effect provided by the support is higher than the heating due to the deposition of a new filament segment. This is due to the large filament diameter being used in the experiments, which produces a relatively large contact with the support.

6.2. Representative results

The sensitivity of the code to small changes in the values of the process parameters was tested by comparing the experimental and theoretical results of temperature evolution while keeping $h_{conv} = 62\ W/m^2\ °C$, $h_{FS} = 250\ W/m^2\ °C$ and $h_{FF} = 50\ W/m^2\ °C$. Fig. 14 corresponds to the condition plotted in Fig. 13, but with a delay of 3 s and 5 s for contact between the two rows (Fig. 14a) and b), respectively). A good agreement between experimental and computational data is observed, even for different extrusion temperatures (not shown): the average and maximum temperature difference between experimental and predicted results was 1.9 °C and 4.8 °C, respectively). The delay in contact influences mainly the temperature of the first segment. When contact between segments is delayed 3 s and 5 s, the temperature of the first segment decreases from 116.7 °C to 102.2 °C and 94.0 °C, respectively. Parallely, the quality of adhesion deteriorates.

The effect of changing the extrusion temperature on the evolution of the filament segment temperature deposited on top (at

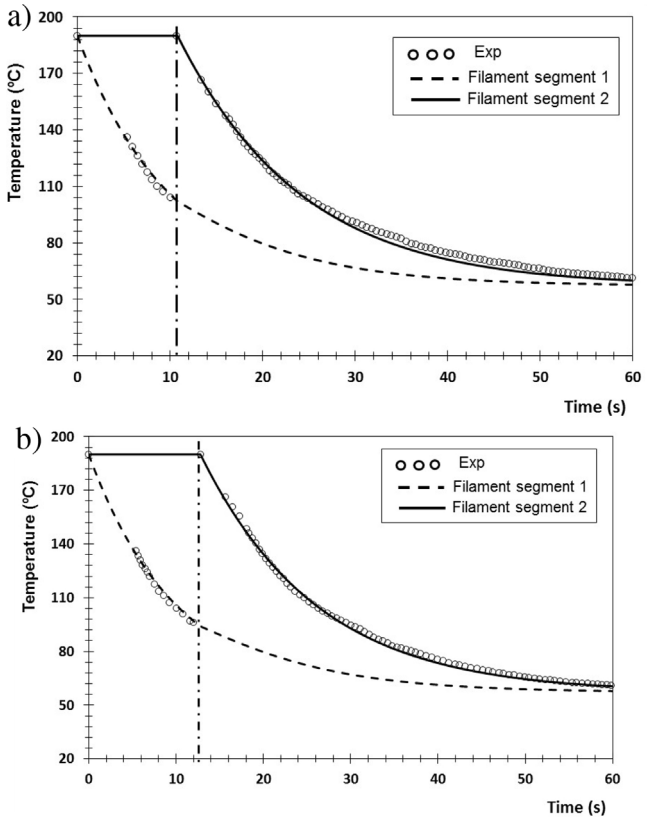

Fig. 14. Evolution of temperature with time (at $x = 40$ mm) of two filament segments deposited on top of each other (same conditions as in Fig. 13), with a delay of mutual contact of: (a) 3 s; (b) 5 s.

$x = 40$ mm) is seen in Fig. 15. A difference of 20 °C in the die set value caused a change of 7 °C in the filament temperature after 60 s. The predictions exhibited values that were generally within 0.4 °C of the measured ones.

Fig. 16 analyses the deposition of a vertical stack of 3 filament segments. The temperatures of the segment on top were again registered at $x = 40$ mm. This cross-section was laid 6.7 s after the equivalent one in the middle and 17.6 s after the one at the bottom. The contact area is important and increases from top to bottom, again due to the large filament diameter used in these experiments.

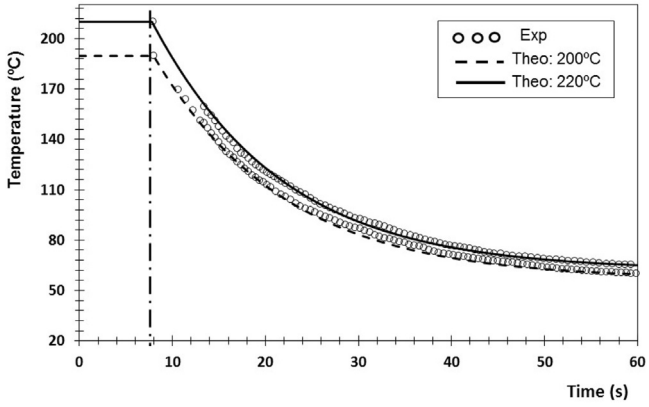

Fig. 15. Temperature evolution with time (at $x = 40$ mm) of a filament segment deposited on top of another (die set to 200 °C and 220 °C).

Temperature readings performed during the deposition of the segment on top are in good agreement with the predictions, which encompassed the entire deposition sequence (on average errors were smaller than 1.3 °C). The Figure also shows that the filament cross-section is essentially circular. In practical FDM, the filament cross-section may become oblong when the size of the filament is higher than the layer thickness value defined by the user (Rodriguez et al., 2003; Gurrala and Regalla, 2014). Due to the need of making measurements, the present study used large filaments that were left free to deform. The deformation of the filament influences the fractions of its perimeter that will contact other segments or the support. This can be easily accommodated in the modeling routine, since these are input values.

6.3. Adhesion

Table 5 reports the relative adhesion strength (in terms of length B_p) for the three deposition patterns illustrated in Fig. 10, for two extrusion temperatures (200 °C and 220 °C). The predicted values were calculated upon identification by the code of the location where the degree of adhesion (defined in Eq. (14)) was smaller than unity (and assuming $h_{conv} = 62\,W/m^2\,°C$, $h_{FS} = 250\,W/m^2\,°C$ and $h_{FF} = 50\,W/m^2\,°C$). The significant standard deviation of the experimental data results from inherent imprecisions of the set-up, such as small oscillations of the extrusion velocity. Nevertheless,

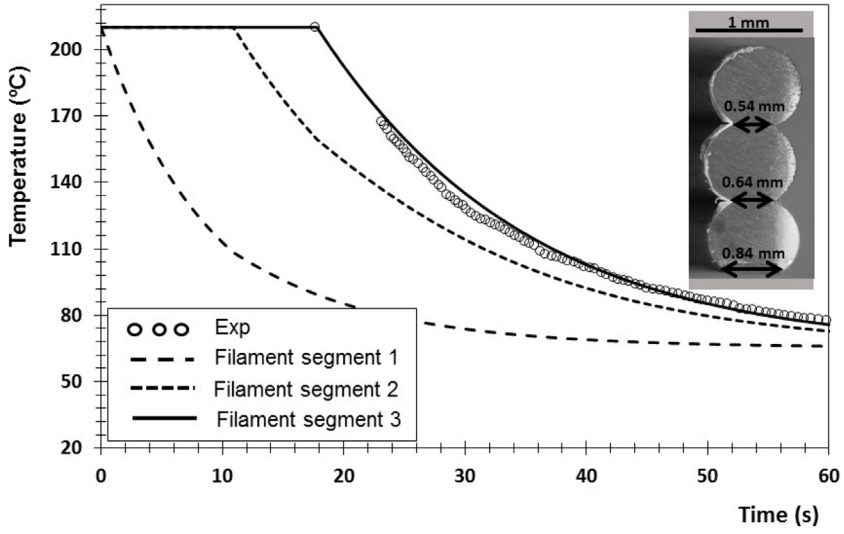

Fig. 16. Temperature evolution with time (at $x = 40$ mm) of a vertical stack of 3 filament segments (die set to 220 °C).

Table 5
Measured and predicted adhesion strength (B_p) of the deposition patterns illustrated in Fig. 10.

Specimen Type	Die @ 200 °C		Die @ 220 °C	
	Predicted B_p (%)	Measured B_p (%)	Predicted B_p (%)	Measured B_p (%)
A	11	8 ± 5	28	23 ± 8
B	0	0 ± 0	13	9 ± 9
C	0	0 ± 0	0	0 ± 0

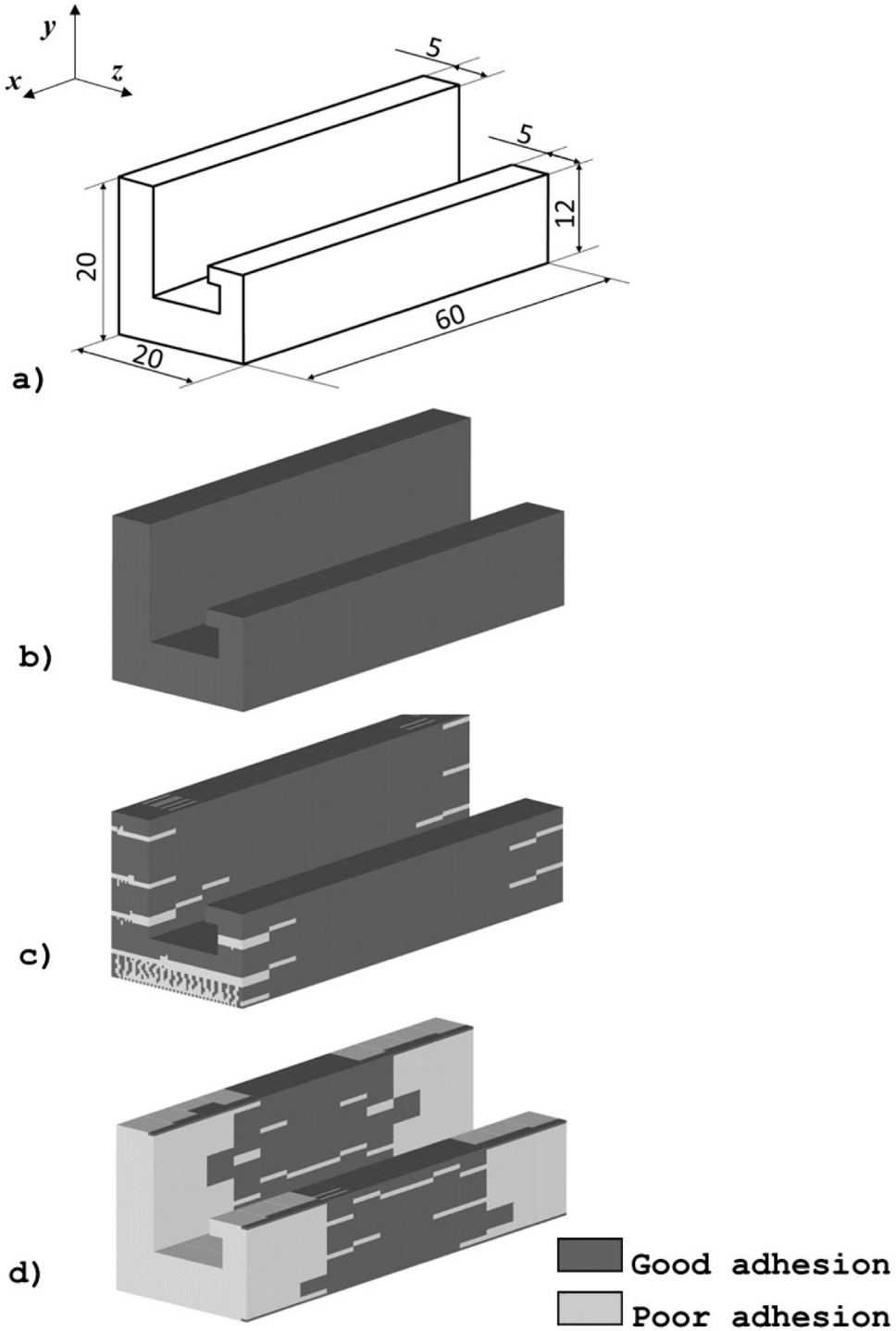

Fig. 17. Effect of the environment temperature on the adhesion of filament segments of a part manufactured by FDT. (a) Geometry of a part to be manufactured by FDT (dimensions in mm; (b) 70 °C; (c) 50 °C; (d) 40 °C).

the qualitative agreement between the two sets of data is quite satisfactory.

As expected, the lower the extrusion temperature the poorest the adhesion. Moreover, since the deposition patterns B and C in Fig. 10 create a gradually higher delay time for the contact between the parallel filament segments relative to pattern A, the corresponding quality of adhesion deteriorates. These results confirm the importance of ensuring sufficient time and temperature between contacting filament segments. In practice, the process may be assisted by pressing the filament onto the deposited portion of the part, this effect being ignored in the present analysis.

6.4. Application example

Since the theoretical predictions are in good agreement with the measurements of filament temperature and adhesion, it seems fitting to demonstrate the use of the computer code for the analysis of a representative part manufactured by FDT. Its geometry and dimensions are shown in Fig. 17. The process parameters and material properties presented in Tables 1 and 2 remain valid, with the exception of the environment temperature, which was changed. The unidirectional and aligned building strategy was adopted. The manufacture of this part could use a second material, to function as support. This would be easily accommodated by the model which, at each location, updates the pertinent material properties. Fig. 17 identifies (in lighter gray) the regions of the part where insufficient adhesion between filament segments is anticipated. These are mostly located at lateral bottom regions, most probably due to the more efficient heat conduction with the environment and with the support. The result shows that decreasing the environment temperature from 70 °C to 50 °C causes about 7% of the entire volume of the part having poor adhesion, while a further decrease to 40 °C raises that value to 52%.

7. Conclusions

This work presented an analytical solution to the transient heat conduction taking place during filament deposition in fused deposition techniques. The analysis is coupled to an algorithm that activates the relevant boundary conditions taking into consideration the deposition sequence. A procedure to compute the adhesion quality between adjacent filament segments was also included in the code. The resulting computational tool considers the main process parameters, such as extrusion velocity, filament dimensions and material, sequence of deposition and environment temperature to predict the evolution of temperature and adhesion during the deposition process and until cooling is completed.

The predictions were experimentally validated both in terms of time evolution of temperature (recorded by thermography) and adhesion (peel-like tests were performed). However, they also demonstrated the need to define carefully the relevant heat transfer coefficients.

Finally, the analysis of a case study demonstrated the usefulness of the method to assist practical operation set-up and optimization.

Acknowledgments

This work was funded by FEDER funds through the COMPETE 2020 Programme and National Funds through FCT – Portuguese Foundation for Science and Technology under the project UID/CTM/50025/2013.

References

Ahn, S.H., Montero, M., Odell, D., Roundy, S., Wright, P.K., 2002. Anisotropic material properties of fused deposition modelling ABS. Rapid Prototyp. J. 8, 248–257.
Bejan, A., 1993. Heat Transfer. John Wiley & Sons, Inc., USA, New York.
Bellini, A., Güçeri, S., 2003. Mechanical characterization of parts fabricated using fused deposition modelling. Rapid Prototyp. J. 9, 252–264.
Bellini, A., Shor, L., Güçeri, S., 2005. New developments in fused deposition modelling of ceramic. Rapid Prototyp. J. 11, 214–220.
Boschetto, A., Bottini, L., 2016. Design for manufacturing of surfaces to improve accuracy in fused deposition modelling. Rob. Comput. Integr. Manuf. 37, 103–114.
Boschetto, A., Giordano, V., Veniali, F., 2013. 3D roughness profile model in fused deposition modelling. Rapid Prototyp. J. 19, 240–252.
Céline, B., Longmei, L., Sunj, Q., Gu, P., 2004. Modelling of bond formation between polymer filaments in the fused deposition modelling process. J. Manuf. Process. 6, 170–178.
Chua, C.K., Leong, K.F., Lim, C.S., 2010. Rapid Prototyping: Principles and Applications. World Scientific.
Costa, S.F., Duarte, F.M., Covas, J.A., 2015. Thermal conditions affecting heat transfer in FDM/FFE: a contribution towards the numerical modelling of the process. Virtual Phys. Prototyp. 10, 35–46.
Croccolo, D., Agostinis, M., Olmi, G., 2013. Experimental characterization and analytical modelling of the mechanical behaviour of fused deposition processed parts made of ABS-M30. Comput. Mater. Sci. 79, 506–518.
Galantucci, L.M., Lavecchia, F., Percoco, G., 2009. Experimental study aiming to enhance the surface finish of fused deposition modelled parts. CIRP Ann. Manuf. Technol. 58, 189–192.
Gurrala, P.K., Regalla, S.P., 2014. Part strength evolution with bonding between filaments in fused deposition modelling. Virtual Phys. Prototyp. 9, 141–149.
Ingole, D.S., Kuthe, A.M., Thakare, S.B., Talankar, A.S., 2009. Rapid prototyping—a technology transfer approach for development of rapid tooling. Rapid Prototyp. J. 15, 280–290.
Kantaros, A., Karalekas, D., 2013. Fiber Bragg grating based investigation of residual strains in ABS parts fabricated by fused deposition modelling process. Mater. Des. 50, 44–50.
Li, L., 2002. PhD Thesis. University of Calgary, Canada.
Masood, S.H., 2014. Advances in fused deposition modelling. In: Hashmi, S. (Ed.), Comprehensive Materials Processing. Elsevier, Amsterdam, pp. 69–91.
Palais, R.S., Palais, R.A., 2009. Differential Equations, Mechanics, and Computation. Providence: American Mathematical Society, USA.
Rodriguez, J.F., Thomas, J.P., Renaud, J.E., 2000. Characterization of the mesostructure of fused-deposition acrylonitrile-butadiene-styrene materials. Rapid Prototyp. J. 6, 175–185.
Rodriguez, J.F., Thomas, J.P., Renaud, J.E., 2003. Design of fused-deposition ABS components for stiffness and strength. J. Mech. Des. 125, 545–551.
Sood, A.K., Ohdar, R.K., Mahapatra, S.S., 2010. Parametric appraisal of mechanical property of fused deposition modelling processed parts. Mater. Des. 31, 287–295.
Sun, Q., Rizvi, G.M., Bellehumeur, C.T., Gu, P., 2008. Effect of processing conditions on the bonding quality of FDM. Rapid Prototyp. J. 14, 72–80.
Sun, Q., 2004. PhD Thesis. University of Calgary, Canada.
Teixeira, P.F., Maia, J., Covas, J., Hilliou, L., 2015. A small-scale experimental extrusion set-up for exploring relationships between process-induced structures and characteristics of multiphase polymer systems. Macromol. Mater. Eng. 300, 1278–1289.
Villalpando, L.H., Eiliat, H., Urbanic, R.J., 2014. An optimization approach for components built by fused deposition modelling with parametric internal structures. Procedia CIRP 17, 800–805.
Yang, F., Pitchumani, R., 2002. Healing of thermoplastic polymers at an interface under nonisothermal conditions. Macromolecules 35, 3213–3224.
Yardimci, M.A., Güçeri, S., 1996. Conceptual framework for the thermal process modelling of fused deposition. Rapid Prototyp. J. 2, 26–31.
Yardimci, M.A., Takeshi, H., Güçeri, S., Danforth, S.C., 1997. Thermal analysis of fused deposition. In: Proceedings in Solid Freeform Fabrication Symposium, Austin, TX, pp. 689–698.